4-6-2014

Tunable Plasmonic and Hyperbolic Metamaterials

Christos Argyropoulos
The University of Texas at Austin

Francesco Monticone
The University of Texas at Austin

Nasim Mohammadi Estrakhri
Chapman University, estakhri@chapman.edu

Andrea Alù
The University of Texas at Austin

Recommended Citation

C. Argyropoulos, F. Monticone, N. Mohammadi Estakhri, and A. Alù, "Tunable Plasmonic and Hyperbolic Metamaterials," International Journal of Antennas and Propagation, Special Issue on 'Reconfigurable Electromagnetics through Metamaterials', Vol. 2014, 532634 (11 pages), April 6, 2014, (invited paper). https://doi.org/10.1155/2014/532634.

Tunable Plasmonic and Hyperbolic Metamaterials

Hindawi Publishing Corporation
International Journal of Antennas and Propagation
Volume 2014, Article ID 532634, 11 pages
http://dx.doi.org/10.1155/2014/532634

Research Article

Tunable Plasmonic and Hyperbolic Metamaterials Based on Enhanced Nonlinear Response

Christos Argyropoulos, Francesco Monticone, Nasim Mohammadi Estakhri, and Andrea Alù

Department of Electrical & Computer Engineering, The University of Texas at Austin, Austin, TX 78712, USA

Correspondence should be addressed to Andrea Alù; alu@mail.utexas.edu

Received 2 December 2013; Accepted 18 February 2014; Published 6 April 2014

Academic Editor: Giacomo Oliveri

We present here tunable and reconfigurable designs of linear and nonlinear plasmonic and hyperbolic metamaterials. Rich scattering features of multilayered composite nanoparticles are demonstrated, which include complex and exotic scattering signatures combining multiple dipolar Fano resonances and electromagnetic induced transparency (EIT) features. These dipole-dipole multi-Fano scattering responses can be further tuned through altering the plasmonic properties of the concentric layers or the permittivity of the core, for instance, by the presence of nonlinearities. Strong third-order nonlinear effects, such as optical bistability, may also be induced in the scattering response of nonlinear nanoparticles due to the highly enhanced and confined fields inside their core. Nonlinear hyperbolic metamaterial designs are also explored, which can realize tunable positive-to-negative refraction at the same frequency, as a function of the input intensity. Negative Goos-Hänchen shift is demonstrated based only on the hyperbolic dispersion properties of these layered metamaterials without the usual need of negative index metamaterials. The Goos-Hänchen shift may be tuned from positive-to-negative values, when the structure is illuminated with different frequencies. A plethora of applications are envisioned based on the proposed tunable metamaterials, such as ultrafast reconfigurable imaging devices, tunable sensors, novel nanotag designs, and efficient all-optical switches and memories.

1. Introduction

Metamaterials are artificially constructed materials that can exhibit novel functionalities not available in nature. Unusual electromagnetic properties, such as negative refraction [1] and invisibility [2, 3], have been achieved with different metamaterial structures. These interesting properties have been obtained with various metamaterial designs at microwaves, terahertz, optical, and ultraviolet frequencies [4–10]. Recently, increased attention has been dedicated to the study of reconfigurable and tunable metamaterials and nonlinear plasmonic devices, where even more exotic and breakthrough functionalities may be achieved [11, 12]. Several reconfigurable and tunable metamaterial and plasmonic devices have been presented in the recent literature. Their operation may be controlled with an applied voltage (varactors) [13, 14], electromagnetic forces [15], external magnetic fields [16], temperature [17, 18], liquid crystals [19, 20], graphene [21, 22], phase-change media [23, 24], and electrooptical effects [25–27].

Nonlinear optical effects can also be strongly enhanced with plasmonic metamaterial structures, mainly due to the highly localized fields obtained in these structures. For example, we recently demonstrated that strong optical bistability can arise when nonlinear plasmonic waveguides operate at their cut-off frequency [28]. Furthermore, inspired by the recent interest in the concept of Fano scattering resonances [29], we reported giant all-optical scattering switches based on nonlinear core-shell plasmonic nanoparticles [30]. The proposed nanoparticles exhibited purely dipolar Fano resonances, in contrast to more conventional Fano resonances based on the interaction and coupling of dipolar and higher-order scattering modes supported by complex subwavelength plasmonic systems [31–35]. The concept of purely dipolar

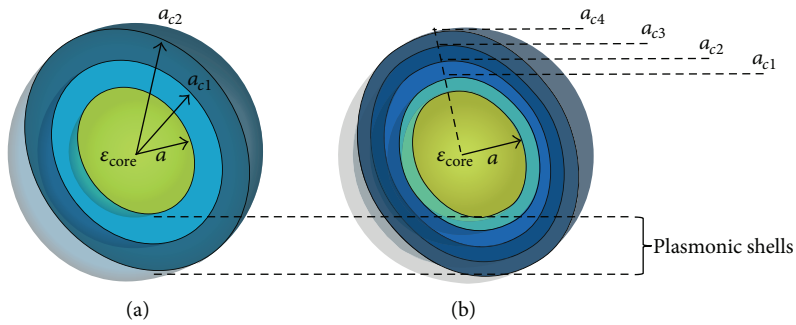

Figure 1: Geometry of composite nanoparticles consisting of (a) two and (b) four plasmonic layers, respectively. The core is made of dielectric material.

Fano resonances has also been extended to multilayered plasmonic nanoparticles, inducing Fano-comb scattering responses [36, 37]. Cloaking and resonant scattering states excited within the proposed plasmonic shells may be used, respectively, as the dark and bright modes to induce multiple dipolar Fano-like scattering features.

In this paper, we further study the interesting scattering properties of multilayered plasmonic nanoparticles in order to demonstrate tunable Fano-comb operation for sensing and nanotagging applications. Third-order optical nonlinear materials loaded in the core of these plasmonic composite nanoparticles are shown to induce large bistability for each dipolar Fano resonance, due to the enhanced and strongly localized electric fields inside the core of the device. Moreover, reconfigurable nonlinear hyperbolic layered metamaterial structures will be studied, which may achieve tunable positive-to-negative refraction as a function of the input radiation intensity [38]. We will also demonstrate that hyperbolic metamaterials can realize strong negative Goos-Hänchen shifts [39] without the need of negative refractive index metamaterials. Reconfigurable operation for Goos-Hänchen shift will be presented based on layered metamaterial structures as a function of the frequency of the impinging radiation.

2. Plasmonic Composite Nanoparticles

Two composite plasmonic nanoparticle geometries are considered in the following, as shown in Figure 1. First, we calculate the scattering response of the geometry depicted in Figure 1(a), consisting of a dielectric core with radius $a = 50\,\text{nm}$ and relative permittivity $\varepsilon_{\text{core}} = 2$ and two plasmonic coating layers. The aspect ratio $\eta_c = a/a_{c1}$ is defined as the ratio between the radius of the dielectric core and the radius of the first plasmonic layer. Both plasmonic layers are considered to have the same thicknesses. The first layer is assumed to follow a lossless Drude permittivity dispersion with $\varepsilon_{c1} = \varepsilon_\infty - \omega_p^2/[\omega(\omega + i\gamma)]$, $\omega_p = 2175\,\text{THz}$, $\gamma = 0\,\text{THz}$, and $\varepsilon_\infty = 5$, fitted to the real part of the experimentally retrieved silver dispersion [40], under an $e^{-i\omega t}$ time convention. The second plasmonic layer has a relative permittivity ε_{c2}, which follows a similar Drude dispersion with a plasma frequency increased by $\Delta\omega_p$. One way to achieve this effect could be to modify the doping level of plasmonic semiconductors, similar to our previous work [37] in which nanoparticles with four plasmonic shells based on aluminum-doped zinc oxide (AZO) semiconductors [41] were utilized to produce Fano scattering combs.

Following the analysis presented in [36], we calculate the quasi-static conditions for resonant scattering and cloaking based on Mie theory [42]. The contour plots of the total SCS of this composite nanoparticle with two plasmonic layers are shown in Figures 2(a)–2(d) as a function of the aspect ratio η_c and the wavelength of operation, where the plasma frequency of the second plasmonic layer is increased by (a) $\Delta\omega_p = 750\,\text{THz}$, (b) $\Delta\omega_p = 500\,\text{THz}$, (c) $\Delta\omega_p = 250\,\text{THz}$, and (d) $\Delta\omega_p = 50\,\text{THz}$ in each case, respectively. The red and blue thick curves in these plots indicate the dispersion of quasi-static conditions for resonant scattering and cloaking, respectively. We fix the geometry picking a large aspect ratio $\eta_c = 0.91$ and calculate the dynamic normalized scattering response (SCS/λ^2), which is shown in Figures 2(e)–2(h) for each increased plasma frequency of the second plasmonic layer. The dimensions of the plasmonic layers are equal to $a_{c1} = a/\eta_c = 55\,\text{nm}$ and $a_{c2} = 60\,\text{nm}$. In Figures 2(e)–2(h) it can be seen that two purely dipolar sharp Fano resonances are formed in the scattering response of the composite plasmonic nanoparticle for different plasma frequencies of the second layer. It is interesting that the second Fano resonance is getting closer to the first as we reduce $\Delta\omega_p$, whereas the first one stays almost unperturbed at the same wavelength position. This demonstrates the high tunability potential of the proposed double-layer nanoparticle design, especially for the second Fano-like resonance.

Next, the same nanoparticle of Figure 1(a) is used, fixing the plasmonic properties of the second layer to be similar to the first layer, but with an increased plasma frequency $\Delta\omega_p = 325\,\text{THz}$. Moreover, the dimensions of the core are changed to $a = 10\,\text{nm}$. The contour plots of the quasi-static SCS are plotted in Figures 3(a)–3(d) as a function of the aspect ratio η_c and of the wavelength of operation, similar to Figure 2, but here the permittivity of the dielectric core

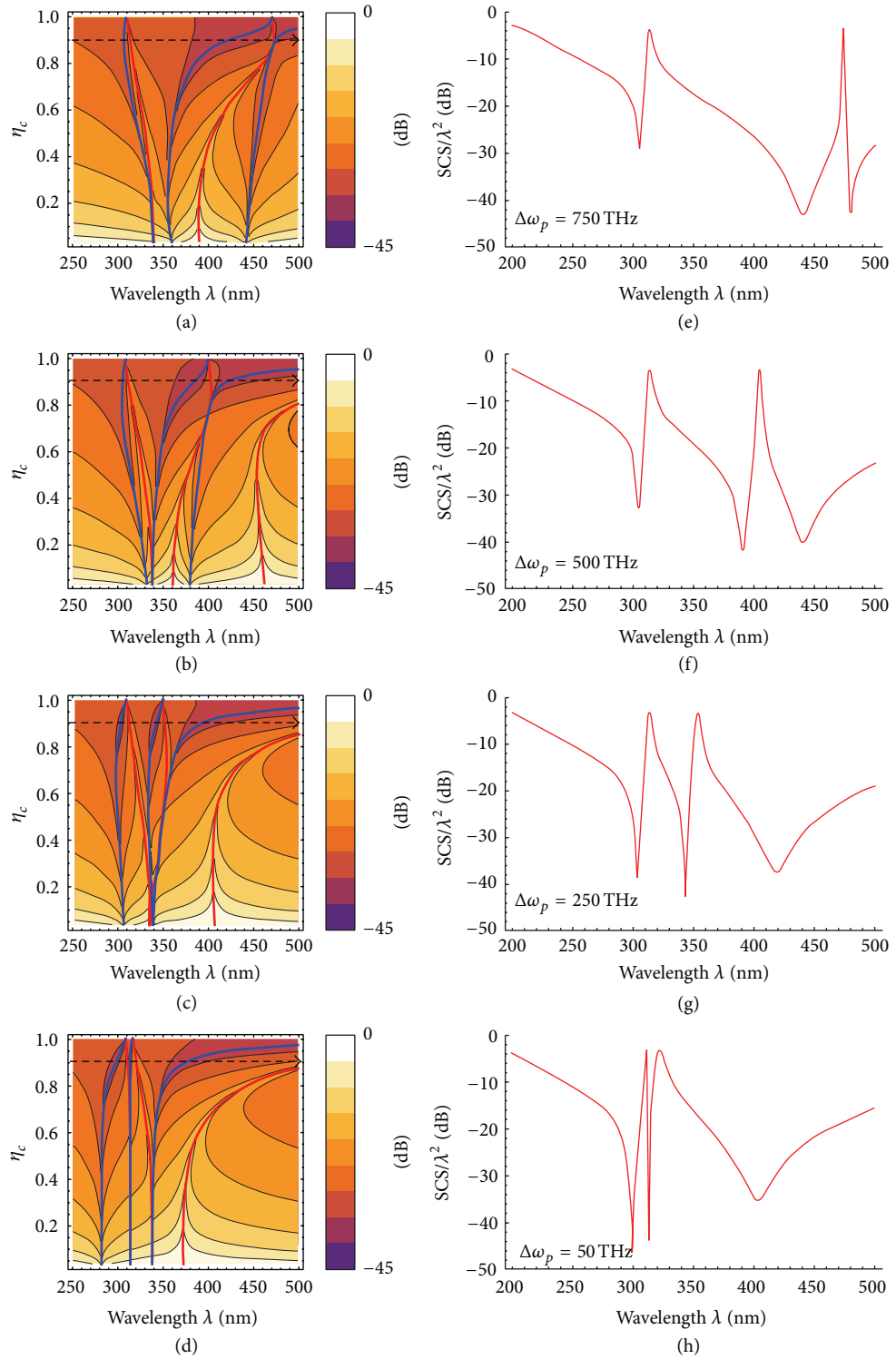

FIGURE 2: (a)–(d) Contour plots of the total SCS (normalized to the maximum value) as a function of the wavelength and the aspect ratio η_c and (e)–(h) normalized SCS/λ^2 versus wavelength, for different plasma frequencies in the two plasmonic layers of the structure in Figure 1(a): (a), (e) $\Delta\omega_p$ = 750 THz, (b), (f) $\Delta\omega_p$ = 500 THz, (c), (g) $\Delta\omega_p$ = 250 THz, and (d), (h) $\Delta\omega_p$ = 50 THz. The aspect ratio is fixed to η_c = 0.91 (indicated by the dashed arrow in panels (a)–(d)). Cloaking (blue lines) and resonant scattering (red lines) quasi-static conditions are also shown in the contour plots (a)–(d).

is different in each case, taking the values (a) $\varepsilon_{\text{core}} = 1.5$, (b) $\varepsilon_{\text{core}} = 4.5$, (c) $\varepsilon_{\text{core}} = 7.5$, and (d) $\varepsilon_{\text{core}} = 10$. Now, a lower aspect ratio is picked, $\eta_c = 0.33$, and the dynamic normalized scattering response (SCS/λ^2) is computed and plotted in Figures 3(e)–3(h) for each permittivity value of the core. In these cases, the dimensions of the plasmonic layers are equal to $a_{c1} = a/\eta_c = 30\,\text{nm}$ and $a_{c2} = 50\,\text{nm}$. Figures 3(e)–3(h) demonstrate that, by changing the core permittivity, we are able to modify and control the frequency positions of both cloaking and resonant scattering states, but selectively tuning only the lower-frequency narrowband Fano resonance. Similar to the previous results, the Fano resonance found at higher frequencies stays fixed, with its shape being unaffected. Hence, tunable operation can also be obtained by changing the core permittivity, leading to reconfigurable Fano scattering responses. Finally, we note that the complex scattering signature shown in Figure 3(h) includes both EIT ($\lambda \cong 450\,\text{nm}$) and Fano responses ($\lambda \cong 350\,\text{nm}$) in the same scattering spectrum. Excitingly, these features can be observed from any angle of observation, due to the purely dipolar nature of the modes involved in these effects. The EIT scattering signature is characterized by a symmetric scattering response, featuring a sharp dip in between two resonant peaks, and it typically arises when two strong resonant states closely interact in frequency. The Fano response, on the contrary, arises when a broad dipolar scattering state, or continuum, interacts with a dark state [29], and it is typically characterized by an asymmetric scattering signature. It is interesting that almost 50 dB scattering contrast, across a very narrow frequency range, may be obtained in the dipolar Fano resonance examples discussed here. Note that the broad cloaking dip shown in Figures 3(e)–3(h) at approximately 300 nm coincides with the "dark" scattering state of the plasmonic cloak [3, 30]. It is based on a single dipolar mode and, quite interestingly, it is weakly affected by the core permittivity values.

The previous examples clearly demonstrate that the degenerate states of cloaking and resonant scattering in composite nanoparticles are tunable and strongly modifiable by just changing the core permittivity. The degeneracy between the two scattering states guarantees strong field enhancement inside the nanoparticle's core at both the cloaking and resonant frequency, which is the ideal condition for enhanced optical nonlinear operation. Now, a double-layer plasmonic composite nanoparticle is considered, with geometry shown in Figure 1(a) and dimensions $a = 3\,\text{nm}$, $a_{c1} = 15\,\text{nm}$, and $a_{c2} = 45\,\text{nm}$. The scattering response of this nanoparticle with core permittivity $\varepsilon_{\text{core}} = 2.2$ is computed and plotted in Figure 4 (blue line) in a narrow wavelength range. This geometry was optimized in order to sustain two closely spaced dipolar Fano resonances with similar shape. The dimensions of the core were chosen to be small in order to further increase the field intensity. The electric field (left insets in Figure 4) and power flow (right insets in Figure 4) distributions are plotted in the E plane at the Fano-like resonant peak (point I, upper insets) and cloaking dip (point II, lower insets), for the first dipolar Fano resonance. As we discussed above, thanks to the degeneracy between cloaking and resonant states, in both cases the fields and power level are enhanced and strongly confined inside and around the dielectric core. Conversely, outside the nanoparticle the field distributions are drastically different: the resonant state causes large scattering around the nanoparticle (point I), whereas at the cloaking wavelength the power flow is almost unperturbed (point II), even right outside of the outer plasmonic layer of the shell.

The strong field enhancement inside the core represents an ideal condition to boost weak optical nonlinear effects. Based on this idea, we propose a nonlinear plasmonic design in which the core is composed of third-order Kerr nonlinear material with permittivity $\varepsilon_{\text{core}} = 2.2 + \chi^{(3)}|E|^2$, where $\chi^{(3)} = 4.4 \times 10^{-20}\,\text{m}^2/\text{V}^2$ is typical value of nonlinear dielectric materials [43] and $|E|$ is the magnitude of the mean value of the local complex electric field in the core of the nanoparticle, calculated using full-wave Mie theory. It is expected that a small change in permittivity of the nonlinear core, induced by an increase in light intensity, will strongly modify the scattering spectrum of the plasmonic nanostructure. The nonlinear scattering response of the proposed nanoparticle is calculated and plotted in Figure 4 (red line), when it is illuminated with a moderate input intensity radiation $I_{\text{in}} = 173\,\text{MW/cm}^2$. Bistable scattering performance is obtained, with broader bistability induced at the second Fano resonance. Both narrowband resonances experience an abrupt switching effect spanning almost 50 dB of total scattering reduction. Note that in this plot we also present the calculated unstable branch indicated by the dashed red line. The nonlinear nanoparticle has a reconfigurable response and its scattering behavior is dependent upon the previous values of input radiation intensities, similar to an optical memory. The scattering signature can switch between different values, which correspond to different branches of the bistability excursion for both dipolar Fano resonances. Hence, the scattering response is characterized by a nonlinear Fano comb with reconfigurable and tunable exotic scattering features. A plethora of potential applications are envisioned based on these nonlinear nanoparticles, such as reconfigurable optical nanotags and tunable sensors.

Next, a four-layer plasmonic composite nanoparticle is analyzed, with geometry shown in Figure 1(b). The relative permittivity of the core is chosen to be $\varepsilon_{\text{core}} = 10$ and its radius is $a = 150\,\text{nm}$. In this case, the plasmonic layers are made of AZO semiconductors with different doping levels. The first plasmonic layer follows a lossless Drude dispersion with relative permittivity $\varepsilon_{c1} = \varepsilon_\infty - \omega_{p1}^2/\omega^2$, where $\varepsilon_\infty = 3.3$ and $\omega_p = 2213\,\text{THz}$ [37]. The other plasmonic layers follow the same Drude dispersion, but assuming different doping levels, leading to an increase in plasma frequency by $\Delta\omega_p$ for each layer, that is, the plasma frequency of each layer will be $\omega_{pn} = \omega_{p1} + (n-1)\Delta\omega_p$, where n is the index of plasmonic layers of the composite nanoparticle. In this case, the aspect ratio η_c is again equal to the ratio between radius of the dielectric core and radius of the first plasmonic layer $\eta_c = a/a_{c1}$. All four plasmonic layers are assumed to have the same thickness.

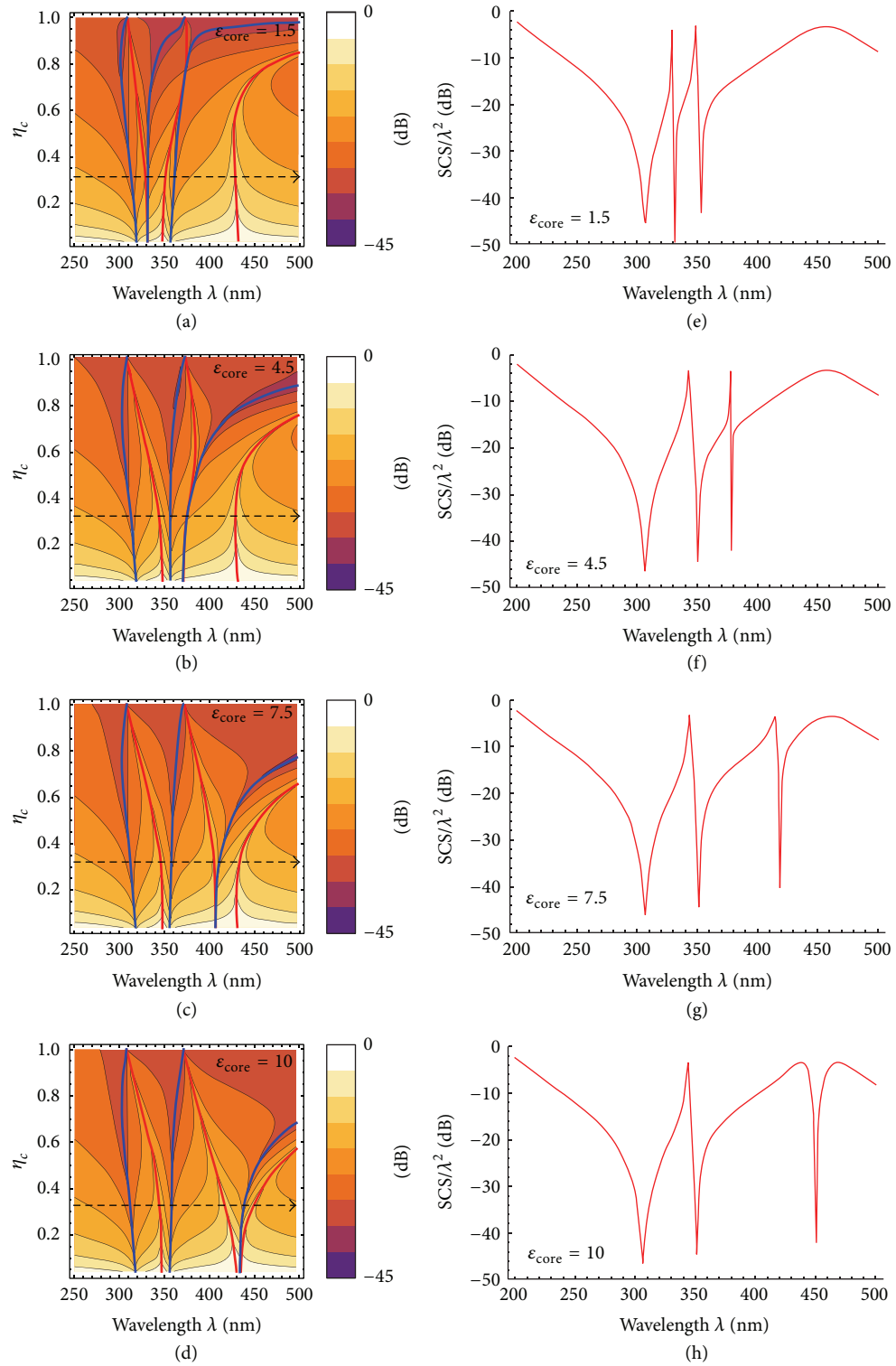

FIGURE 3: (a)–(d) Contour plots of the total SCS (normalized to the maximum value) as a function of the wavelength and the aspect ratio η_c and (e)–(h) normalized SCS/λ^2 versus wavelength, for different core permittivities of the structure in Figure 1(a): (a), (e) ε_{core} = 1.5, (b), (f) ε_{core} = 4.5, (c), (g) ε_{core} = 7.5, and (d), (h) ε_{core} = 10. The aspect ratio is fixed to η_c = 0.33 (indicated by the dashed arrow in panels (a)–(d)). Cloaking (blue lines) and resonant scattering (red lines) quasi-static conditions are also shown in the contour plots (a)–(d).

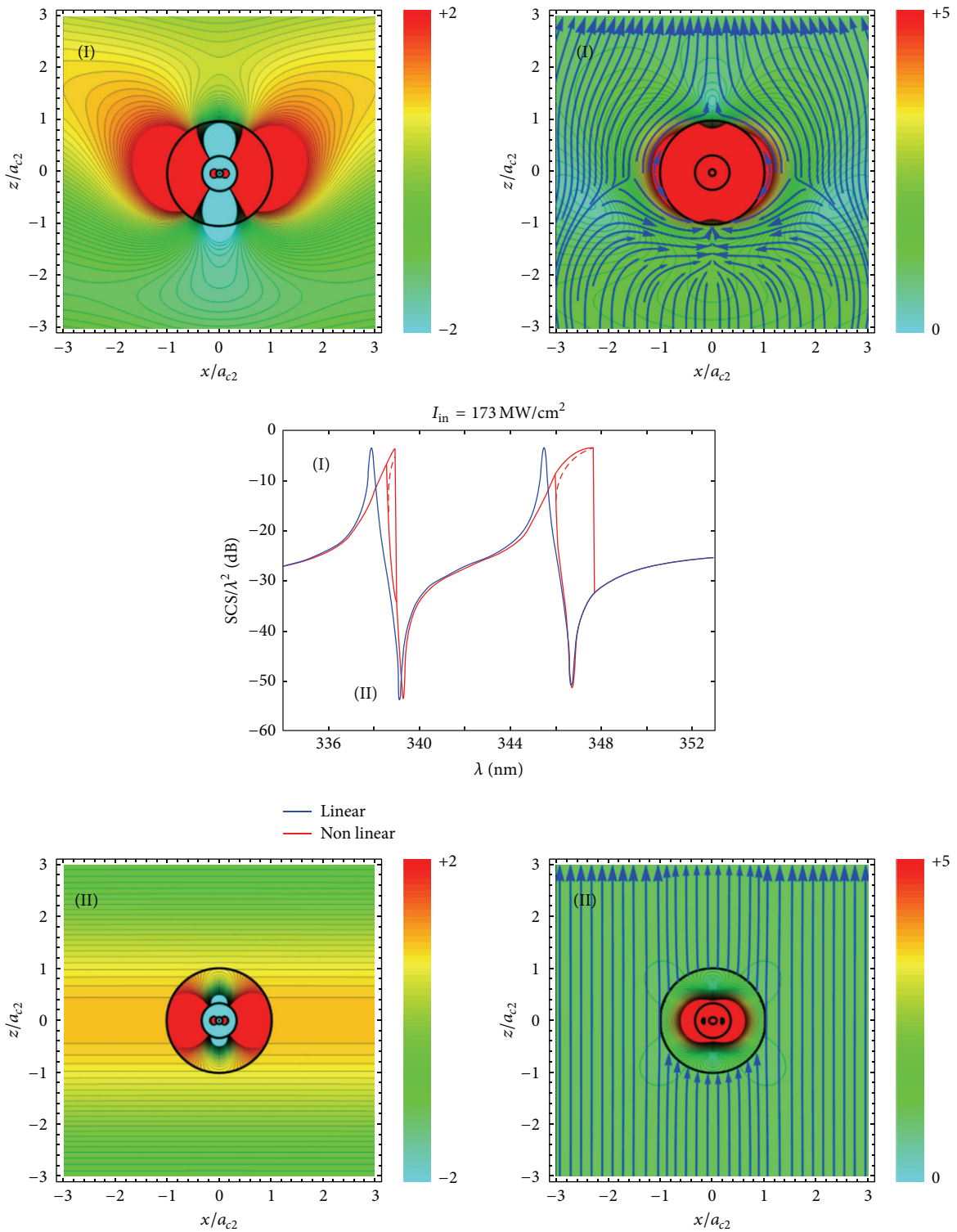

FIGURE 4: Normalized scattering response versus wavelength, for linear (blue line) and nonlinear (red line) dielectric core for the geometry in Figure 1(a). The electric field (left insets) and power flow (right insets) distributions are plotted on the E plane at the higher-frequency Fano-like resonant peak (I) and cloaking dip (II) when linear operation is considered. The nonlinear plasmonic nanoparticle is illuminated with input intensity I_{in} = 173 MW/cm^2. The unstable branch of the nonlinear bistable response is plotted with a dashed red line.

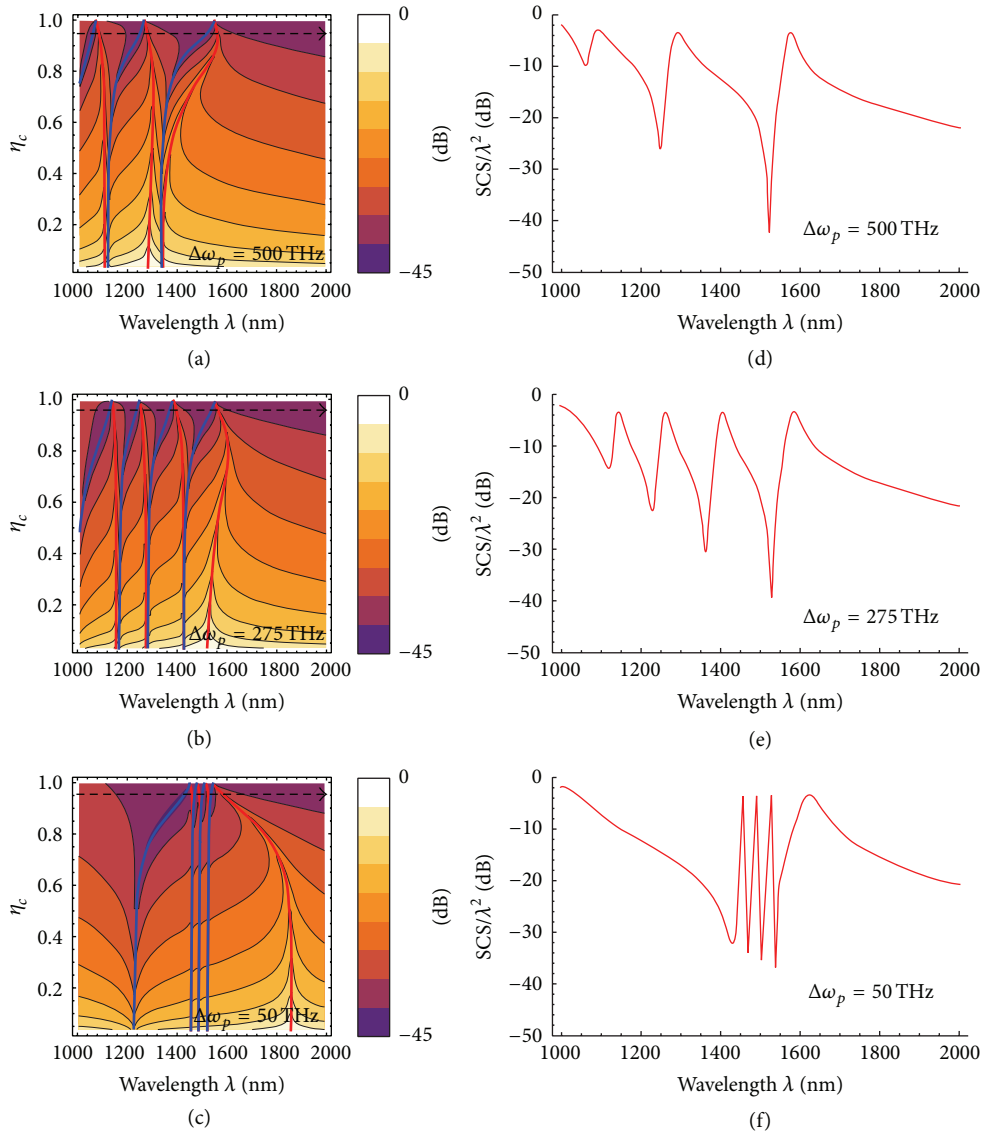

FIGURE 5: (a)–(c) Contour plots of the total SCS (normalized to the maximum value) as a function of wavelength and aspect ratio η_c. (d)–(f) normalized SCS/λ^2 versus wavelength, for different plasma frequencies in the four plasmonic layers of the geometry of Figure 1(b): (a), (d) $\Delta\omega_p$ = 500 THz, (b), (e) $\Delta\omega_p$ = 275 THz, and (c), (f) $\Delta\omega_p$ = 50 THz. The aspect ratio is fixed in these cases to η_c = 0.952 (indicated by the dashed arrow in panels (a)–(c)). Cloaking (blue lines) and resonant scattering (red lines) quasi-static conditions are also shown in the contour plots (a)–(c).

Applying Mie theory consistent to the analysis presented in [37], we calculate the quasi-static conditions for resonant scattering and cloaking states of each dipolar Fano resonance. The contour plots of the total SCS of this four-layer plasmonic composite nanoparticle are shown in Figures 5(a)–5(c) as a function of the aspect ratio η_c and the wavelength of operation, and the plasma frequency of each plasmonic layer is increased by (a) $\Delta\omega_p$ = 500 THz, (b) $\Delta\omega_p$ = 275 THz, and (c) $\Delta\omega_p$ = 50 THz, respectively. Rich and exotic scattering spectra are obtained for this multilayered plasmonic nanoparticle, with multiple dipolar Fano resonances (Fano-comb scattering signature). The dynamic normalized scattering response (SCS/λ^2) is calculated for a large aspect ratio η_c = 0.952 and plotted in Figures 5(d)–5(f) for different plasma frequencies of each plasmonic layer. The dimensions of the four plasmonic layers are equal to $a_{c1} = a/\eta_c$ = 157.5 nm, a_{c2} = 165 nm, a_{c3} = 172.5 nm, and a_{c4} = 180 nm. Multiple purely dipolar sharp Fano resonances can be seen in Figures 5(d)–5(f), creating a Fano-comb scattering response. Note that the narrowband Fano resonances, produced at near infrared wavelengths, get closer together as we reduce $\Delta\omega_p$, whereas the broader conventional dipolar resonance stays almost unperturbed at the same wavelength position λ = 1650 nm. Hence, tunable Fano comb scattering signatures

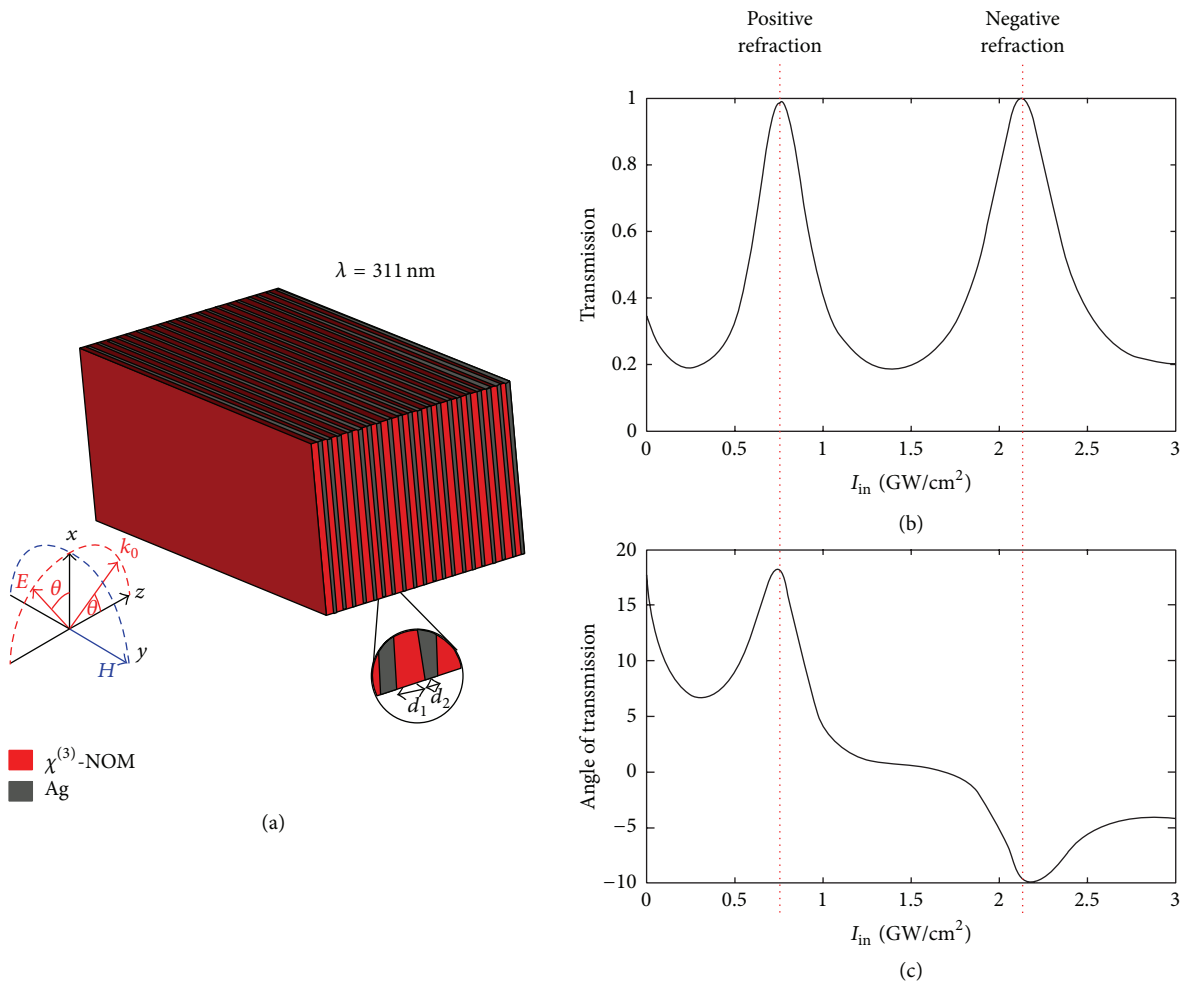

FIGURE 6: (a) Geometry of a nonlinear hyperbolic metamaterial with tunable response. (b) Transmittance and (c) angle of transmission (in degrees) as a function of the input intensity for the structure shown in panel (a), with third-order Kerr nonlinearity introduced in the dielectric layers. The results are computed for incident radiation wavelength of $\lambda = 311$ nm.

may be obtained as we modify the doping levels of the semiconductor material used for each plasmonic layer of the composite nanoparticle. Reconfigurable optical tagging applications may be achieved with these multilayer nanoparticle designs, exhibiting tunable scattering response based on the doping level of each plasmonic semiconductor shell.

3. Hyperbolic Metamaterials

In the following, we study tunable and reconfigurable effects in hyperbolic metamaterial structures. The geometry of the layered nonlinear metamaterial structure is shown in Figure 6(a). The structure may be characterized as an inhomogeneous anisotropic slab composed of 20 alternating layers of Kerr-nonlinear dielectric material and lossless plasmonic silver (Ag). The thicknesses of both layers are subwavelength with values $d_1 = 50$ nm and $d_2 = 25$ nm, respectively. The dispersion of the plasmonic Ag material is modeled by a Drude permittivity $\varepsilon_{Ag} = \varepsilon_\infty - \omega_p^2/\omega^2$, where $\omega_p = 2175$ THz and $\varepsilon_\infty = 5$, based on the experimental data retrieved from [40]. The third-order nonlinear dielectric material has a relative permittivity $\varepsilon_d = \varepsilon_L + \chi^{(3)}|E|^2$, where $\varepsilon_L = 0.1$ and $\chi^{(3)} = 4.4 \times 10^{-18}$ m^2/V^2, a common value for semiconductor nonlinear materials [43]. The nonlinear permittivity directly depends on the local electric field inside the nonlinear layers induced by the incident radiation intensity. This device is characterized by hyperbolic dispersion and, as a result, negative refraction without requiring a negative refractive index may be obtained over a relatively broad frequency range, as shown in [38].

The structure is illuminated by a monochromatic plane wave operating at $\lambda = 311$ nm and at an incidence angle $\theta_i = 45^\circ$. The transmittance and the angle of transmission (relative to normal direction), varying the input radiation intensity, are plotted in Figures 6(b) and 6(c), respectively. Two peaks in transmission (Figure 6(b)) are obtained at two different input intensities: $I_{in} = 0.78$ GW/cm^2 and $I_{in} = 2.1$ GW/cm^2. These peaks correspond to positive and negative angles of the transmitted wave, as seen in Figure 6(c). The response of

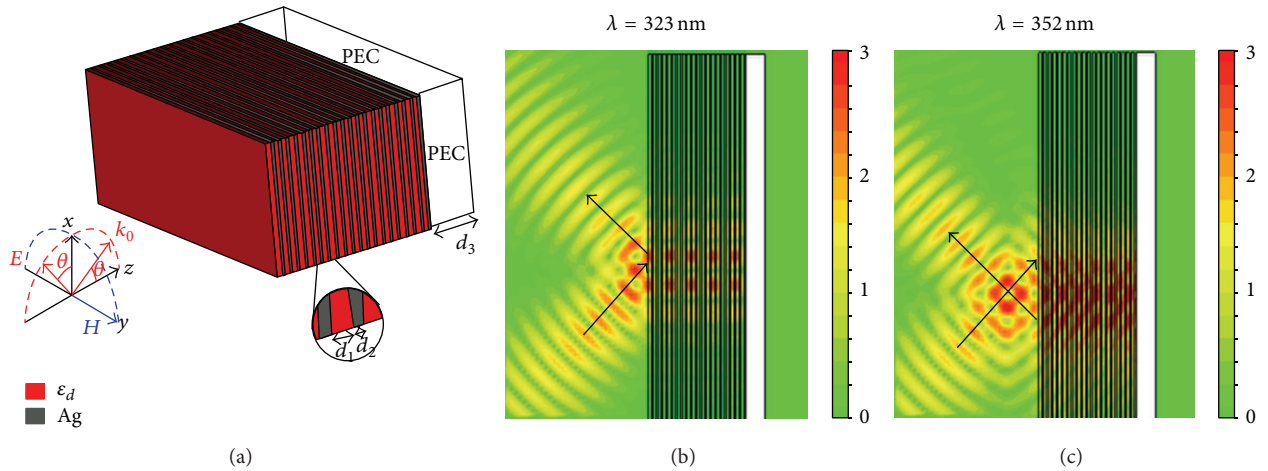

FIGURE 7: (a) Geometry of a hyperbolic metamaterial terminated by a PEC (mirror) slab with thickness $d_3 = 300$ nm. Tunable (b) positive and (c) negative Goos-Hänchen shifts obtained at two different illumination wavelengths: $\lambda = 323$ nm and $\lambda = 352$ nm, respectively.

the layered nonlinear hyperbolic metamaterial may drastically change, as we increase the input intensity, from positive to negative refraction at the same frequency. Hence, tunable and reconfigurable refraction may be achieved as a function of the input radiation intensity.

Next, a different layered hyperbolic metamaterial is studied, terminated this time by a perfect electric conductor (PEC), operating as a mirror for electromagnetic waves. The geometry of this structure is shown in Figure 7(a). In this case, the transmission is equal to zero and only reflected waves exist. The layers are now composed of dielectric material with relative permittivity $\varepsilon_d = 2$ and thickness $d_1 = 50$ nm and silver with the same Drude dispersion described before and thickness $d_1 = 25$ nm. The PEC slab is used to terminate the layered metamaterial and has thickness $d_3 = 300$ nm. The back mirror may be realized with different metals, which approximate the PEC properties at optical frequencies when their thickness is much larger than their skin depth ($\delta \approx 30$ nm).

The Goos-Hänchen shift [39] of the reflected wave from this structure is analyzed for two different wavelengths of operation. Figure 7(b) demonstrates the operation of this device at $\lambda = 323$ nm, when negative refraction is not realized inside the hyperlens. It can be seen that the Goos-Hänchen shift is positive and rather small at this frequency point, as it is expected for the usual operation of conventional dielectrics, which refract light in a positive way. However, when the device is illuminated at $\lambda = 352$ nm, strong negative Goos-Hänchen shift is obtained, which is clearly shown in Figure 7(c). This effect causes a distinctively strong focal spot of radiation in front of the hyperbolic metamaterial. The negative shift is a direct outcome of the negative refraction the waves experience inside the hyperlens, which is dominant and strong for this particular frequency point. Moreover, this effect can arise without the usual requirements of negative refractive index metamaterials. It is interesting that hyperbolic metamaterials may also lead to "trapped rainbow" configurations with lower losses compared to devices based on double negative metamaterials [44]. To sum up, tunable Goos-Hänchen shift, positive to negative, may be obtained with the same hyperbolic metamaterial as a function of the frequency of operation. With the addition of proper nonlinearity or tunable materials, it may be also possible to induce these effects at the same frequency of operation.

4. Conclusions

To conclude, we have presented here tunable and reconfigurable plasmonic metamaterial designs using linear and nonlinear materials. Multilayered plasmonic composite nanoparticles have been demonstrated to achieve exotic and complex scattering responses, which may be tuned at will, as we change the doping level of the semiconductor layers or the permittivity of the dielectric core. Dipolar Fano resonances, EIT-like effects, and Fano scattering combs have been obtained based on these composite nanoparticles. Their scattering response may be further reconfigured when Kerr nonlinear materials are included in their core, leading to strong optical bistability, all-optical switching, and memory operation. Furthermore, layered hyperbolic metamaterials have been studied considering third-order nonlinear materials introduced in their layers. Tunable operation with positive-to-negative refraction has been demonstrated as the input radiation intensity is increased. Finally, reconfigurable Goos-Hänchen shift has been presented in a linear layered hyperbolic metamaterial. The shift may change from positive to negative when the same metamaterial structure is illuminated at different frequencies. The proposed sharp Fano scattering signatures and the negative refraction properties of the proposed hyperbolic metamaterial are expected to be affected when realistic losses are included in the metallic parts [36–38]. Nevertheless, gain and active media may be in principle introduced in the dielectric layers [38], expectedly compensating the inherent metallic losses. The incorporation of gain and active materials

holds the promise to bridge the gap towards viable applications of the proposed devices. To sum up, novel linear and nonlinear metamaterial and plasmonic designs have been presented here with large potential for ultrafast all-optical data processing. Numerous applications may be envisioned based on the proposed devices, such as tunable sensors or nanotags, as well as reconfigurable subwavelength imaging systems.

Conflict of Interests

The authors declare that there is no conflict of interests regarding the publication of this paper.

Acknowledgments

This work has been partially supported by the ARO STTR project "Dynamically Tunable Metamaterials," AFOSR with the YIP Award no. FA9550-11-1-0009, and the ONR MURI Grant no. N00014-10-1-0942.

References

[1] D. R. Smith, J. B. Pendry, and M. C. K. Wiltshire, "Metamaterials and negative refractive index," *Science*, vol. 305, no. 5685, pp. 788–792, 2004.

[2] J. B. Pendry, D. Schurig, and D. R. Smith, "Controlling electromagnetic fields," *Science*, vol. 312, no. 5781, pp. 1780–1782, 2006.

[3] A. Alù and N. Engheta, "Achieving transparency with plasmonic and metamaterial coatings," *Physical Review E: Statistical, Nonlinear, and Soft Matter Physics*, vol. 72, Article ID 016623, 2005.

[4] R. A. Shelby, D. R. Smith, and S. Schultz, "Experimental verification of a negative index of refraction," *Science*, vol. 292, no. 5514, pp. 77–79, 2001.

[5] S. Linden, C. Enkrich, M. Wegener, J. Zhou, T. Koschny, and C. M. Soukoulis, "Magnetic response of metamaterials at 100 terahertz," *Science*, vol. 306, no. 5700, pp. 1351–1353, 2004.

[6] D. Rainwater, A. Kerkhoff, K. Melin, J. C. Soric, G. Moreno, and A. Alù, "Experimental verification of three-dimensional plasmonic cloaking in free-space," *New Journal of Physics*, vol. 14, Article ID 013054, 2012.

[7] J. Valentine, J. Li, T. Zentgraf, G. Bartal, and X. Zhang, "An optical cloak made of dielectrics," *Nature Materials*, vol. 8, no. 7, pp. 568–571, 2009.

[8] L. H. Gabrielli, J. Cardenas, C. B. Poitras, and M. Lipson, "Silicon nanostructure cloak operating at optical frequencies," *Nature Photonics*, vol. 3, no. 8, pp. 461–463, 2009.

[9] D. Bao, K. Z. Rajab, Y. Hao et al., "All-dielectric invisibility cloaks made of $BaTiO_3$-loaded polyurethane foam," *New Journal of Physics*, vol. 13, Article ID 103023, 2011.

[10] C. Argyropoulos, F. Monticone, G. D'Aguanno, and A. Alù, "Plasmonic nanoparticles and metasurfaces to realize Fano spectra at ultraviolet wavelengths," *Applied Physics Letters*, vol. 103, no. 14, Article ID 143113, 2013.

[11] N. I. Zheludev and Y. S. Kivshar, "From metamaterials to metadevices," *Nature Materials*, vol. 11, no. 11, pp. 917–924, 2012.

[12] M. Kauranen and A. V. Zayats, "Nonlinear plasmonics," *Nature Photonics*, vol. 6, no. 11, pp. 737–748, 2012.

[13] B. Wang, J. Zhou, T. Koschny, and C. M. Soukoulis, "Nonlinear properties of split-ring resonators," *Optics Express*, vol. 16, no. 20, pp. 16058–16063, 2008.

[14] D. Huang, E. Poutrina, and D. R. Smith, "Analysis of the power dependent tuning of a varactor-loaded metamaterial at microwave frequencies," *Applied Physics Letters*, vol. 96, no. 10, Article ID 104104, 2010.

[15] M. Lapine, I. V. Shadrivov, D. A. Powell, and Y. S. Kivshar, "Magnetoelastic metamaterials," *Nature Materials*, vol. 11, no. 1, pp. 30–33, 2012.

[16] B. Ozbey and O. Aktas, "Continuously tunable terahertz metamaterial employing magnetically actuated cantilevers," *Optics Express*, vol. 19, no. 7, pp. 5741–5752, 2011.

[17] V. A. Fedotov, A. Tsiatmas, J. H. Shi et al., "Temperature control of Fano resonances and transmission in superconducting metamaterials," *Optics Express*, vol. 18, no. 9, pp. 9015–9019, 2010.

[18] W.-X. Huang, X.-G. Yin, C.-P. Huang, Q.-J. Wang, T.-F. Miao, and Y.-Y. Zhu, "Optical switching of a metamaterial by temperature controlling," *Applied Physics Letters*, vol. 96, no. 26, Article ID 261908, 2010.

[19] Q. Zhao, L. Kang, B. Du et al., "Electrically tunable negative permeability metamaterials based on nematic liquid crystals," *Applied Physics Letters*, vol. 90, no. 1, Article ID 011112, 2007.

[20] X. Wang, D.-H. Kwon, D. H. Werner, I.-C. Khoo, A. V. Kildishev, and V. M. Shalaev, "Tunable optical negative-index metamaterials employing anisotropic liquid crystals," *Applied Physics Letters*, vol. 91, no. 14, Article ID 143122, 2007.

[21] N. Papasimakis, Z. Luo, Z. X. Shen et al., "Graphene in a photonic metamaterial," *Optics Express*, vol. 18, no. 8, pp. 8353–8359, 2010.

[22] H. Yan, X. Li, B. Chandra et al., "Tunable infrared plasmonic devices using graphene/insulator stacks," *Nature Nanotechnology*, vol. 7, pp. 330–334, 2012.

[23] T. Driscoll, H.-T. Kim, B.-G. Chae et al., "Memory metamaterials," *Science*, vol. 325, no. 5947, pp. 1518–1521, 2009.

[24] K. Appavoo and R. F. Haglund Jr., "Detecting nanoscale size dependence in VO_2 phase transition using a split-ring resonator metamaterial," *Nano Letters*, vol. 11, no. 3, pp. 1025–1031, 2011.

[25] H.-T. Chen, J. F. O'Hara, A. K. Azad et al., "Experimental demonstration of frequency-agile terahertz metamaterials," *Nature Photonics*, vol. 2, no. 5, pp. 295–298, 2008.

[26] H. Tao, A. C. Strikwerda, K. Fan, W. J. Padilla, X. Zhang, and R. D. Averitt, "Reconfigurable terahertz metamaterials," *Physical Review Letters*, vol. 103, no. 14, Article ID 147401, 2009.

[27] Z. L. Samson, K. F. MacDonald, F. de Angelis et al., "Metamaterial electro-optic switch of nanoscale thickness," *Applied Physics Letters*, vol. 96, Article ID 143105, 2010.

[28] C. Argyropoulos, P. Y. Chen, G. D'Aguano, N. Engheta, and A. Alù, "Boosting optical nonlinearities in epsilon-near-zero plasmonic channels," *Physical Review B*, vol. 85, no. 4, Article ID 045129, 2012.

[29] B. Luk'Yanchuk, N. I. Zheludev, S. A. Maier et al., "The Fano resonance in plasmonic nanostructures and metamaterials," *Nature Materials*, vol. 9, no. 9, pp. 707–715, 2010.

[30] C. Argyropoulos, P. Y. Chen, F. Monticone, G. D'Aguanno, and A. Alù, "Nonlinear plasmonic cloaks to realize giant all-optical scattering switching," *Physical Review Letters*, vol. 108, no. 26, Article ID 263905, 2012.

[31] F. Hao, Y. Sonnefraud, P. van Dorpe, S. A. Maier, N. J. Halas, and P. Nordlander, "Symmetry breaking in plasmonic nanocavities: subradiant LSPR sensing and a tunable Fano resonance," *Nano Letters*, vol. 8, no. 11, pp. 3983–3988, 2008.

[32] S. Zhang, D. A. Genov, Y. Wang, M. Liu, and X. Zhang, "Plasmon-induced transparency in metamaterials," *Physical Review Letters*, vol. 101, no. 4, Article ID 047401, 2008.

[33] N. Liu, L. Langguth, T. Weiss et al., "Plasmonic analogue of electromagnetically induced transparency at the Drude damping limit," *Nature Materials*, vol. 8, no. 9, pp. 758–762, 2009.

[34] J. A. Fan, C. Wu, K. Bao et al., "Self-assembled plasmonic nanoparticle clusters," *Science*, vol. 328, no. 5982, pp. 1135–1138, 2010.

[35] F. Shafiei, F. Monticone, K. Q. Le et al., "A subwavelength plasmonic metamolecule exhibiting magnetic-based optical Fano resonance," *Nature Nanotechnology*, vol. 8, pp. 95–99, 2013.

[36] F. Monticone, C. Argyropoulos, and A. Alu, "Layered plasmonic cloaks to tailor the optical scattering at the nanoscale," *Scientific Reports*, vol. 2, pp. 912–918, 2012.

[37] F. Monticone, C. Argyropoulos, and A. Alu, "Multi-layered plasmonic covers for comb-like scattering response and optical tagging," *Physical Review Letters*, vol. 110, no. 11, Article ID 113901, 2013.

[38] C. Argyropoulos, N. M. Estakhri, F. Monticone, and A. Alù, "Negative refraction, gain and nonlinear effects in hyperbolic metamaterials," *Optics Express*, vol. 21, no. 12, pp. 15037–15047, 2013.

[39] F. Goos and H. Hänchen, "Ein neuer und fundamentaler versuch zur totalreflexion," *Annalen der Physik*, vol. 436, no. 7-8, pp. 333–346, 1947.

[40] P. B. Johnson and R. W. Christy, "Optical constants of the noble metals," *Physical Review B*, vol. 6, no. 12, pp. 4370–4379, 1972.

[41] G. V. Naik, J. Kim, and A. Boltasseva, "Oxides and nitrides as alternative plasmonic materials in the optical range," *Optical Material Express*, vol. 1, no. 6, pp. 1090–1099, 2011.

[42] C. F. Bohren and D. R. Huffman, *Absorption and Scattering of Light by Small Particles*, John Wiley & Sons, New York, NY, USA, 1983.

[43] R. W. Boyd, *Nonlinear Optics*, Academic Press, London, UK, 1992.

[44] K. L. Tsakmakidis, A. D. Boardman, and O. Hess, "'Trapped rainbow' storage of light in metamaterials," *Nature*, vol. 450, no. 7168, pp. 397–401, 2007.